A&A 490, 365–375 (2008)
DOI: 10.1051/0004-6361:200809994

Astronomy & Astrophysics

Surface characterization of Pluto and Charon by L and M band spectra

S. Protopapa[1], H. Boehnhardt[1], T. M. Herbst[2], D. P. Cruikshank[3], W. M. Grundy[4], F. Merlin[5], and C. B. Olkin[6]

[1] Max-Planck Institute for Solar System Research, Max-Planck-Str. 2, 37191 Katlenburg-Lindau, Germany
e-mail: [protopapa;boehnhardt]@mps.mpg.de
[2] Max Planck Institute for Astronomy, Königstuhl 17, 69117 Heidelberg, Germany
e-mail: herbst@mpia.de
[3] NASA Ames Research Center, Mail Stop 245-6, Moffett Field, CA 94035, USA
e-mail: Dale.P.Cruikshank@nasa.gov
[4] Lowell Observatory, 1400 W. Mars Hill Rd., Flagstaff, AZ 86001, USA
e-mail: w.grundy@lowell.edu
[5] LESIA, Observatoire de Paris, 92195 Meudon Principal Cedex, France
e-mail: frederic.merlin@obspm.fr
[6] Department of Space Studies, Southwest Research Institute, Boulder, CO, USA
e-mail: colkin@boulder.swri.edu

Received 17 April 2008 / Accepted 8 July 2008

ABSTRACT

Context. One of the main scientific objectives of NASA's New Horizons mission is to map the icy surface compositions of Pluto and its moon Charon. The encounter will be in 2015. Meanwhile remote observations from earth and space are the most suitable means to enhance further our knowledge of the Pluto/Charon system.
Aims. We intend to assist the New Horizons mission by improving our knowledge of Pluto's and Charon's surface compositions. Specifically, we extend the wavelength coverage of the surface spectroscopy beyond the *K* band, with the goal to detect further surface ice absorption bands predicted from the models that are based on the available *JHK* spectra, and to search for signatures of yet unknown ices. In particular we aim to resolve the binary system Pluto/Charon and to obtain, for the first time, spectra up to 5 μm of the two objects resolved.
Methods. Spectroscopic measurements of Pluto/Charon taken with the adaptive optics instrument NACO at the ESO VLT in the interval 3–7 August 2005 were obtained. The nature and properties of the compounds present on the surface of Pluto and Charon are investigated by applying a Hapke radiative transfer model to the measured spectra.
Results. We present Pluto's reflectance spectrum in the wavelength range (1–5) μm. Apart from known and expected absorption bands of methane ice, our Pluto spectrum reveals a new absorption band centered near 4.6 μm, not previously detected. This absorption band could be related to the presence of CO and nitriles (compounds of C and N connected with a triple bond). A geographic mixture of pure methane ice with two different grain sizes, methane and CO ice diluted in nitrogen, CH_2CHCN and titan tholin gives the best fit to Pluto's spectrum, although not in all details. Differences compared to published Pluto spectra from 2001 taken at similar longitude could be due to a different surface coverage in latitude or to a possible resurfacing process on Pluto. Charon's spectrum is measured in the wavelength range (1–4) μm. The surface of Charon can be modeled by pure water ice darkened by a spectrally neutral continuum absorber.

Key words. Kuiper Belt – techniques: spectroscopic – methods: numerical – scattering

1. Introduction

Beyond the orbit of Neptune there exists a population of bodies that is a remnant from the formation of the Solar System; this is called the Kuiper belt, or the Trans-neptunian objects (TNOs). Scientific interest in these bodies arises because they are considered representatives of the most pristine Solar System objects observable from Earth. Improving the knowledge of these distant bodies extends the understanding of the origin and evolution of the Solar System.

Pluto, now considered a dwarf planet, plays a key role in the study of Kuiper Belt objects (KBOs). It is the name-giving representative of the Plutino population in the Kuiper Belt (TNOs in 2:3 mean motion resonance with Neptune) and the first example of what are now known to be abundant binary and multiple systems in the Kuiper Belt. In terms of surface composition, Pluto appears to be the most prominent representative of the large ($r \gtrsim 750$ km) KBOs like Eris (Brown et al. 2005; Licandro et al. 2006a; Dumas et al. 2007; Merlin et al. 2007), 2005 FY9 [newly named Makemake] (Licandro et al. 2006b; Brown et al. 2007; Tegler et al. 2007, 2008), Sedna (Barucci et al. 2005) and Triton (Quirico et al. 1999), which is generally thought to be a large TNO captured by Neptune. Like Pluto (Owen et al. 1993; Douté et al. 1999), these objects have infrared spectra dominated by CH_4 ice absorptions. Wavelength shifts of these absorption bands relative to those of pure CH_4 ice, detected in the infrared and/or visible spectra, suggest that part of the CH_4 on the surface is dissolved in another ice. Much of what we understand of the

Table 1. Observing geometry of the Pluto-Charon system for our VLT/NACO measurements in August 2005. The UT time corresponding to the first (UT_{start}) and last (UT_{end}) Pluto/Charon spectrum is reported. α is the Sun-(Pluto-Charon) barycenter-Earth (phase) angle. Ob-lon and Ob-lat are the apparent planetographic longitude and latitude of the center of Pluto's disk seen by the observer. In particular the apparent planetographic longitude of the first and last Pluto spectrum acquired in the same night are given. Light travel-time target-observer is taken into account. AM is the airmass interval between the first and last Pluto spectrum acquired in the same night. PA and PARANG are position angle and parallactic angle, respectively. The table lists the interval between the values of PA and PARANG of the first and last Pluto spectrum acquired in the same night.

UT_{start}	UT_{end}	α (deg)	Ob-lon (deg)	Ob-lat (deg)	AM	PA (deg)	PARANG (deg)	seeing ($''$)
2005 August 04 02:07	2005 August 04 05:55	1.44	7÷16	–34	1.03÷2.44	173÷–173	131÷111	0.8–2.2
2005 August 04 23:40	2005 August 05 04:55	1.46	58÷70	–34	1.09÷1.66	–129÷–121	–117÷110	0.6–1.2
2005 August 05 23:46	2005 August 06 05:46	1.48	114÷128	–34	1.07÷2.43	–94÷–85	–120÷111	0.5–1.2
2005 August 06 23:28	2005 August 07 05:54	1.50	170÷185	–34	1.10÷2.70	–37÷–11	–116÷111	0.6–1.0

physical constitution, composition and evolution of the objects in the Kuiper Belt is put into context by Earth-based studies of Pluto, since it is one of the few objects bright enough for detailed measurements.

In 2006, NASA launched its New Horizons spacecraft to Pluto and its moons, the first probe ever targeting a dwarf planet in the outer Solar System. One of the main scientific objectives of NASA's New Horizons mission is to map the icy surface composition of Pluto and Charon and to assess and analyse the likely temporary atmosphere of the dwarf planet, an enigmatic phenomenon not yet found in other TNOs. The encounter will be in 2015. Meanwhile remote observations from earth and space are the most suitable means to further enhance our knowledge of the Pluto/Charon system.

In the past, the *L*- and *M*-band regions were notoriously under-exploited for outer Solar System studies, because of the low reflectivities of Solar System materials coupled with the weak solar flux, complications due to strong telluric absorptions and a lack of adequate instrumentation. However, longer wavelengths offer several potential advantages since the fundamental vibrational transitions of many ice species are located in this region and the absorptions are much stronger than the those observed shortward of 2.5 μm. The importance of *L*- and *M*-band spectroscopy derives also from the fact that New Horizons instruments will perform spectroscopy of Pluto's surface in the *JHK* bands only. Hence, the observations presented in this paper will complement the information coming from New Horizons. The first attempt to investigate Pluto's *L*-band was done by Spencer et al. (1990) and then revisited by Grundy et al. (2002a) and by Olkin et al. (2007). While Charon's spectrum was never measured beyond 2.5 μm, Olkin et al. (2007) combined spectra of the unresolved Pluto-Charon system obtained from the Keck and Subaru telescopes from 2.8 to 4.2 μm with 0.8–2.4 μm spectra from the NASA Infrared Telescope Facility, and proposed as a possible surface scenario for Pluto a geographic mixture of pure CH_4, CH_4 diluted in N_2 and tholin. This result was obtained after modeling and removing the contribution of Charon from the measured reflectance spectra. Since there are no measured Charon-only spectra beyond 2.5 μm, it was assumed for the model spectra that were used instead, that the same H_2O ice and spectrally neutral continuum absorber that dominates Charon's spectrum at shorter wavelengths (Buie & Grundy 2000) is dominant beyond 3 μm as well.

In this paper we present results from spectroscopic observations of the Pluto-Charon system performed at the European Southern Observatory (ESO) Chile, covering the wavelength range (1–5) μm for Pluto and (1–4) μm for Charon. The compositions, properties and distribution of the ices present on the surface of Pluto and its moon Charon are investigated using the radiative transfer model of Hapke.

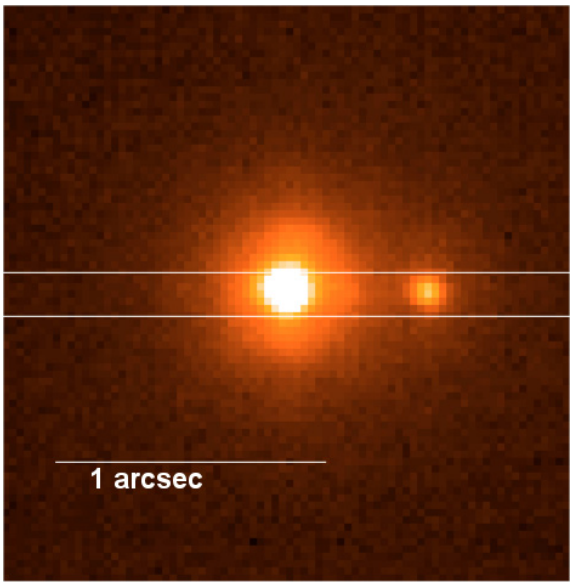

Fig. 1. Median averaged slit acquisition image of Pluto (on the left in the image) and Charon (on the right in the image) in the night 4 August 2005. The NACO slit is indicated in the figure by two horizontal white lines.

2. Observations and data reduction

We present spectroscopic measurements of Pluto/Charon obtained with the NACO instrument at the ESO VLT during the interval 3–7 August 2005. NACO (see www.eso.org/instruments/naco/), at the VLT Unit Telescope 4 (Yepun), consists of the Nasmyth Adaptive Optics System (NAOS; AO for adaptive optics) and the High Resolution infrared (IR) Camera and Spectrometer (CONICA). The AO system resolved Pluto-Charon and enabled us to benefit from considerable signal to noise improvements for the spectroscopy. Using the NACO prism L27_P1 we covered the complete wavelength range (1–5) μm simultaneously with a spectral resolution of 35 in *J* band and 200 in *M* band. The observational circumstances are listed in Table 1.

The Pluto-Charon binary was used as a reference source for the visible AO sensor of NACO. The slit (width 172 mas) was set along the orbital position angle of the system, in order to acquire Pluto and Charon simultaneously (see Fig. 1). The slit acquisition was performed in *K*-band and a suitable offset correction, depending on the zenith distance, was applied in order to achieve the optimum slit centering of the objects for *L* and *M* bands. This approach slightly sacrificed the *JHK* signal of the objects, at least for higher airmasses, because of slit losses due to differential atmospheric refraction. The observations were

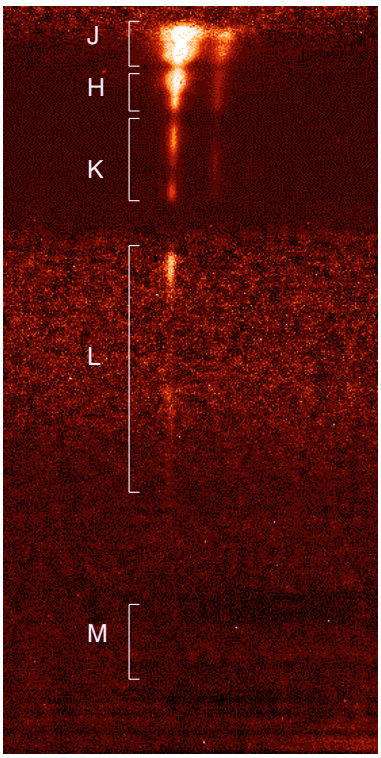

Fig. 2. Bidimensional spectrum of Pluto/Charon system acquired in the night 5 August 2005 at airmass 1.60. In the image, Pluto is on the left, Charon on the right and the wavelength bands are indicated along the *y* axis.

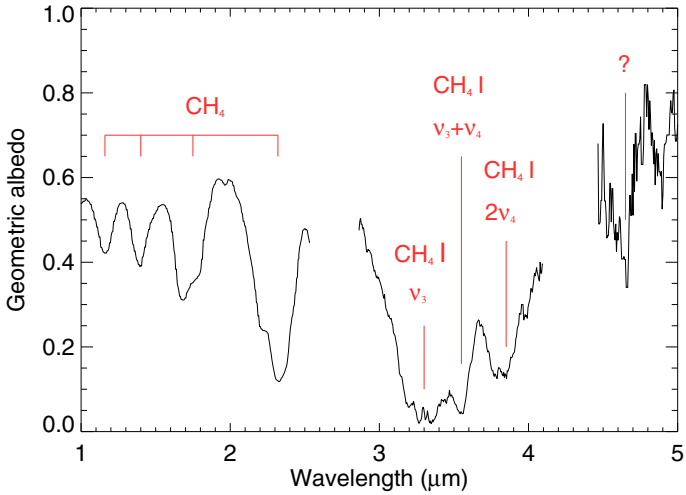

Fig. 3. Pluto's spectrum in the wavelength range (1–5) μm. The species responsible for the absorption bands detected in Pluto's spectrum are marked in the figure. No object flux is measured in the atmospheric absorption bands at 2.50–2.86 and 4.10–4.46 μm.

performed using the usual A-B-B-A nodding (with some jitter) along the slit. Spectra of the nearby solar analog star HD 162341 (G2/G3V), recorded approximately every 1.5 h, were obtained in order to remove simultaneously both the telluric and solar features from the Pluto and Charon spectra. In this way each Pluto-Charon observation had an associated set of "before" and "after" calibration star observations acquired under similar sky conditions and for identical instrument and AO settings.

Besides the usual data reduction for IR spectroscopy (background subtraction, flat fielding, ABBA spectra co-addition, removing telluric and solar features), special attention was paid to wavelength calibration and spectrum curvature removal of the NACO data. The former was difficult since arc lamp spectra are not available to calibrate the strongly non-linear dispersion of the prism. Indeed, at long wavelengths there are no visible arc lines, while at short wavelengths the lines are severely blended. Hence, atmospheric emission and absorption features were used as wavelength reference. The spectrum curvature results from differential atmospheric refraction (see Fig. 2) over the large wavelength range, and was corrected by pixel shifts of the spectra applying the atmospheric refraction formula (Szokoly 2005). Thereafter, we used optimum extraction of the spectra to improve the signal-to-noise ratio over the aperture extraction (Horne 1986). Finally, the spectra acquired in the second and last nights of observations were averaged, due to their better quality, especially in the *L*- and *M*-bands, compared to those of the other two nights (see Table 1). Indeed, the spectroscopic measurements acquired in the first night of observations suffer from bad seeing conditions, with seeing up to 2.2″ (see Table 1), and operational problems. Most of the observations obtained in the third night are affected by electronic noise in the *L*- and *M*-range of the detector. In particular, groups of spectra for each target object were combined, eliminating spurious data arising from defects in individual exposures. In order to minimize light losses in the short wavelength region (due to atmospheric refraction), we obtained the final spectra of Pluto and Charon by averaging the *JHK* spectra obtained at low values of airmass ($AM \leq 1.23$). In the *L*- and *M*-bands we averaged all of the useful spectra taken up to a maximum airmass of 2.47 in the *L*-band and 1.25 in *M*-band. The extracted spectra were normalized using published values for the geometric albedo at fixed wavelengths. Specifically, Pluto's spectrum was normalized in the wavelength range (1.9–2.1) μm to 0.57, a value extracted from the Pluto IRTF spectrum of Olkin et al. (2007). The IRTF spectrum was scaled to the HST/NICMOS spectrum of Pluto (Grundy & Buie 2002). Using this normalization, the averaged *L*- and *M*-band geometric albedo of Pluto are in agreement with Spitzer results (Emery, private communication). Charon was normalized in the range (2.2–2.3) μm to 0.31, according to the HST/NICMOS Charon's spectrum by Buie & Grundy (2000). The spectra were binned using a wavelength step $\delta\lambda = 0.005$ μm. In Figs. 3 and 4 we present the NACO reflectance spectra obtained for Pluto and Charon, respectively. In the wavelength range (1.0–2.5) μm the standard deviation (STD) of Pluto's and Charon's spectra is around 0.04 and 0.01 respectively, while it increases in the range 1.80–1.95 μm due to the presence of strong lines of telluric H_2O. In the *L* band, from 3.1 to 4.0 μm, the STD is about 0.05 for Pluto and 0.09 for Charon. These values increase at the atmospheric band edges due to the strong telluric absorptions. In the *M* band, between 4.6 and 4.7 μm the STD of Pluto has values around 0.15, much smaller than at the edges of the band.

3. Spectroscopic analysis

In this section we present a qualitative description of the Pluto and Charon spectra, focusing attention on both the known compounds and unknown features. The quantitative analysis of the spectra will be described in the subsequent section.

3.1. Pluto

Published spectra of Pluto in the wavelength range (1.0–4.2) μm have established the presence of CH_4 ice on Pluto's surface,

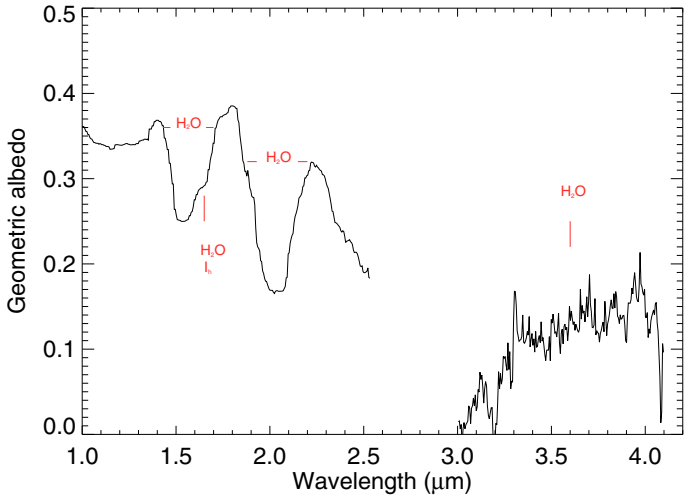

Fig. 4. Charon's spectrum in the wavelength range (1.0–4.1) μm. No object flux is measured in the atmospheric absorption bands at 2.5–3.0 μm. The species responsible for the absorption bands detected in Charon's spectrum are marked in the figure.

identified first by Cruikshank et al. (1976). This is confirmed by our NACO results. Indeed, in the wavelength range (1.0–2.5) μm the spectrum is dominated by prominent CH_4 features at 1.16, 1.40, 1.67, 1.79, 2.20 and 2.32 μm (Fig. 3). Also the *L*-band spectrum (2.9–4.1) μm is characterized by CH_4 absorption bands around 3.30, 3.55 and 3.80 μm corresponding to ν_3, $\nu_2+\nu_4$ and $2\nu_4$ vibrational transitions (Grundy et al. 2002a; Olkin et al. 2007). Because of the low spectral resolution of the NACO prism, it is not possible to detect the CO ice absorption bands at 1.579 and 2.354 μm (Owen et al. 1993; Douté et al. 1999) and the N_2 feature at 2.149 μm first seen by Owen et al. (1993). The low spectral resolution in the *JHK* bands does not allow differentiation between pure CH_4 and CH_4 diluted in N_2, which can be distinguished spectroscopically by a small shift in the peak frequencies of the bands (Quirico & Schmitt 1997), as first seen in the spectrum of Triton (Cruikshank et al. 1993). From laboratory measurements by Quirico & Schmitt (1997) of CH_4 diluted in β N_2 at 44 K compared with those of pure CH_4 at 43.5 K, this shift varies, in the wavelength range (1–2.5) μm, from 0.003 to 0.005 μm. A shift of this magnitude is smaller than or comparable to the wavelength bin (selected to match the minimum resolution of the prism), so it is undistinguishable in the data.

Our NACO spectrum reveals the presence of a previously unknown and thus unidentified absorption band around 4.6 μm, indicated by a question mark in Fig. 3. This absorption, a first detection at the limit of the instrumental capability that must be confirmed by further observations, could be related to the presence of CO ice on Pluto's surface. Indeed, CO ice displays an absorption band around 4.67 μm (Palumbo & Strazzulla 1993) in laboratory spectra. Also, CO ice is known to be present on the surface of the dwarf planet from the short wavelength region (Douté et al. 1999; Owen et al. 1993), with highest abundance on the anti-Charon hemisphere (Grundy & Buie 2001). Another possible explanation for the 4.6 μm feature is the presence of nitriles on Pluto. Nitriles are organic compounds characterized by a triple bond connecting carbon and nitrogen. They are predicted to precipitate to the surface in photochemical models of Pluto's atmosphere (Krasnopolsky & Cruikshank 1999). The nitrile band near 4.6 μm varies somewhat in position, depending on the environment in which the molecule occurs and the other atom or functional groups attached to the C-atom on the side opposite the N-atom (Cruikshank et al. 1991). Several nitriles, in pure form, have been studied in laboratory (dello Russo & Khanna 1996; Masterson & Khanna 1990) like acetonitrile (CH_3CN), propionitrile (CH_3CH_2CN), acrylonitrile (CH_2CHCN), hydrogen cyanide (HCN), cyanogen (C_2N_2), cyanoacetylene (HC_3N), dicyanoacetylene (C_4N_2) and cyanopropyne (CH_3C_3N), presenting (at 35 K) absorption bands at 4.450 μm, 4.506 μm, 4.488 μm, 4.843 μm, 4.619 μm, 4.405 μm, 4.454 μm, 4.396 μm, respectively. The 4.6 μm absorption band in Pluto's spectrum could be a blend of more than one individual molecular species. However, we do not have information about the form in which nitriles might occur on Pluto's surface, whether in pure form or diluted in a nitrogen matrix.

3.2. Charon

Figure 4 shows the NACO spectrum of Charon, the first one measured also in the *L* band. The spectrum confirms the presence on Charon's surface of H_2O ice, by the absorption bands at 1.5 and 2.0 μm, together with the 1.65 μm feature diagnostic of crystalline water ice (Brown & Calvin 2000). Because of the low spectral resolution it is not possible to detect in the NACO spectrum the 2.21 μm feature attributed to hydrated ammonia (Cook et al. 2007).

From the presence of strong absorption bands of H_2O ice in the short wavelength region, it is not surprising that a very broad water ice signature is found in the *L* band part of Charon's surface spectrum.

4. Modeling

A quantitative analysis of the Pluto and Charon spectra was performed using the scattering radiative transfer model of Hapke (1993). In order to model the observed reflectance spectra of Pluto and Charon and to extract, in this way, information about their surface composition, an IDL routine was developed. This routine computes the bidirectional reflectance of a geographical or an intimate mixture $r(i, e, g)$ once the optical constants of the assumed surface ices of the mixture together with the geometry of the system (incident angle i, emission angle e and phase angle g) are known. The opposition effect and large-scale roughness are considered, together with anisotropic scattering. This latter factor is taken into account by considering the Henyey-Greenstein particle phase function

$$p(g) = \frac{1-\xi^2}{(1+2\xi\cos g+\xi^2)^{3/2}} \quad (1)$$

where ξ is the cosine asymmetry factor (Hapke 1993). Following the approach by Olkin et al. (2007), the spherical body of the target is approximated by a 30×30 bi-dimensional grid of surface elements, and for each surface element incident angle and emission angle (i_k, e_k) are computed. The geometric albedo of the target, A_p, that will be compared with the observations is then determined using the following relation

$$A_p = \frac{\pi \sum_{k=1}^{N} r(i_k, e_k, g)\cos e_k}{N} \quad (2)$$

where N is the total number of surface elements covering the visible disk of the body. We simulated the albedo at small, non-zero phase angles corresponding to the phase angles typically observed from Earth. The free parameters in our model are grain size and contribution of each surface terrain to the mixture. They

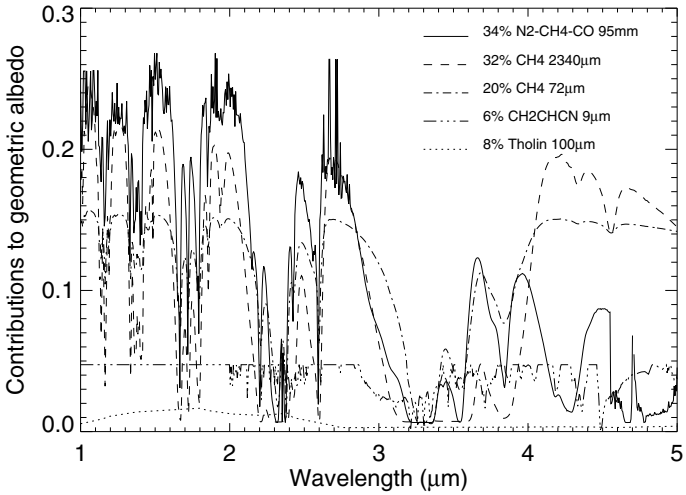

Fig. 5. Contributions of each model terrain to Pluto's geometric albedo spectrum.

are iteratively modified by means of a χ^2 minimization algorithm (Levenberg-Marquardt least-squares minimization) until a best fit to the observations is achieved. For the cosine asymmetry parameter (ξ), the compaction parameter (h) and the mean roughness slope (θ) we considered values known from previous studies (Hillier et al. 1994; Olkin et al. 2007; Buie & Grundy 2000). Sections 4.1 and 4.2 describe the results obtained from modeling the Pluto and Charon spectra, respectively.

4.1. Pluto

Because of the low spectral resolution of NACO spectrum in *JHK* bands and the light losses due to differential atmospheric refraction in *J*- and *H*- bands (see Sect. 2), IRTF observations of Pluto obtained in 2002 (Olkin et al. 2007) at high spectral resolution over the wavelength range (1.0–2.4) μm were combined with the NACO spectrum of Pluto in the *L*- and *M*-bands to be used as input for the modeling. The best-fitting model of this composite Pluto spectrum was obtained with a five-terrain unit model consisting of 32% of pure CH_4 at 60 K (optical constants from Grundy et al. 2002b) with 2340 μm grain size, 20% of CH_4 at 60 K with 72 μm grains, 34% of CH_4 and CO ice diluted in N_2 (CH_4:CO:N_2) at 41 K with 95 mm grains, 6% of CH_2CHCN (optical constants at 35 K from dello Russo & Khanna 1996) with 9 μm grains (the limiting case, since the grain size is approaching the wavelength of the radiation) and 8% of titan tholin (optical constants from Khare et al. 1984) at 100 μm grains. The concentration of CH_4 and CO in N_2 are 0.36% and 0.1%, respectively. The optical constants of CH_4:CO:N_2 were obtained as described by Douté et al. (1999), using the optical constants of pure N_2 and CH_4 diluted in N_2 derived by Quirico et al. (1996) and Quirico & Schmitt (1997), respectively. The CO ice optical constants were taken from Schmitt et al. (1992) in the wavelength range from 1.43 to 2.5 μm and from Ehrenfreund et al. (1996) (30 K) in the wavelength range from 4.55 to 5 μm. Following the approach of Olkin et al. (2007) we assumed a cosine asymmetry factor ξ equal to –0.3. Buie et al. (1997) showed Pluto's phase coefficient to be nearly identical to that of Triton, and –0.3 is the ξ value found by Voyager for Triton (Hillier et al. 1994). The values assumed for surface roughness and compaction parameter are 14°, by analogy with Triton, and 0.5 (Olkin et al. 2007), respectively. The contribution to Pluto's geometric albedo of each single terrain considered in the modeling is shown in Fig. 5. In the range between 1 and 2 μm we assumed the reflectance spectrum of CH_2CHCN to be flat, since the optical constants of dello Russo & Khanna (1996) cover the wavelength range 2–5 μm only. Figure 6 shows the comparison between Pluto's spectrum (solid line) and our best fit model (dashed line). This model may not be a unique solution and depends on the surface components considered. Figure 7 shows the comparison between the averaged NACO spectrum (solid line) together with its standard deviation (STD) as function of wavelength (dash dot dot dot lines) in the range (1–2.5) μm and the best fit model (dashed line) degraded to the same spectral resolution as the NACO observations. This was done by convolving the high spectral resolution model shown in Fig. 6 with a Gaussian profile with FWHM (Full Width at Half Maximum) of 0.05 μm in the (1–2.5) μm wavelength range corresponding to a spectral resolution of 35. The synthetic spectrum reproduces all the main features of the observed spectrum, although not in all details. The deviation of the model from the observed spectrum is within the errors, although the model deviates from the observations in the continuum regions around 1.0, 1.3 and 1.5 μm. The reason for this deviation is the light loss of NACO spectrum due to the atmospheric refraction. The comparison between the IRTF observations of Pluto obtained in 2002 (Olkin et al. 2007) at high spectral resolution (see Fig. 8) and the modeled spectrum suggests that our model reproduces correctly the measured depths of the CH_4 absorption bands. The presence of CH_4 diluted in N_2 reproduces the nitrogen absorption band at 2.149 μm and takes into account the coexistence of pure and diluted methane at the surface of Pluto (Douté et al. 1999). Difficulties in fitting the albedo at 2.32 and 2.37 μm arise because of the saturation of the CH_4 absorption bands at these wavelengths. This problem was solved by including CH_2CHCN and titan tholin as continuum scatterers. In the short wavelength region acrylonitrile, as well as titan tholin, displays an high, almost neutral geometric albedo which increases the reflectance around 2.32 and 2.37 μm. Figure 9 shows the averaged NACO spectrum (solid line) together with its standard deviation (STD) as function of wavelength (dash dot dot dot lines) compared with our best-fit model (dashed line) in the range (2.9–4.1) μm. It is possible to verify that the deviation of the model from the observed spectrum in the *L*-band is within the errors, although with systematic deviations depending on wavelength.

The comparison between the NACO and Keck (Olkin et al. 2007) observations obtained in 2005 and 2001, respectively, is also shown. The main difference between the two sets of data is the spectral slope between 2.9 and 3.1 μm. The NACO spectrum presents, even considering the STD, a slope that is steeper than that observed in 2001. This spectral difference can be due to viewing geometry since geographical regions at different longitudes and latitudes come into view. The NACO spectrum was obtained by averaging the spectra acquired in the second and last night of observations (see Sect. 2), corresponding to a sub-Earth longitude of 64° and 178°, respectively (see Table 1). The spectra of the two opposite hemispheres of Pluto do not show any significant difference (the variation is inside the STD) in the wavelength range between 2.9 and 3.7 μm (see Fig. 10). This evidence, together with the fact that Keck spectrum refers to a sub-Earth longitude of 198°, near the one covered by NACO on 7 August 2005, makes longitudinal changes in the ice composition very unlikely as reason for the slope difference between NACO and Keck spectra. The spectral change between NACO and Keck data might be compatible with variations in the observed surface latitude. Another possible explanation for the spectral difference between NACO and Keck spectra is the temporal change

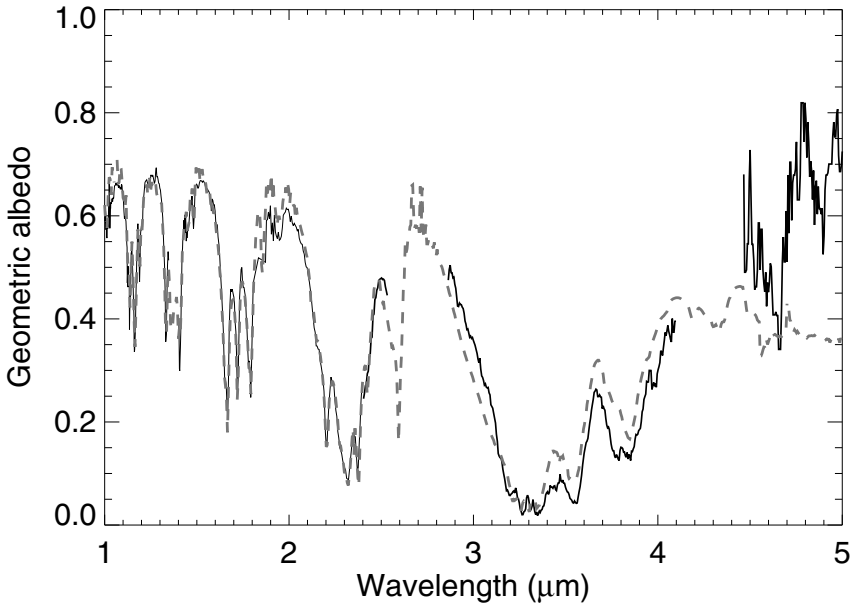

Fig. 6. Pluto's spectrum (solid line) obtained by combining the 2002 IRTF observations (Olkin et al. 2007) at high spectral resolution over the wavelength range (1.0–2.4) μm and the NACO spectrum in *L*- and *M*-band is shown. Overplotted is the best-fitting model (dashed curve).

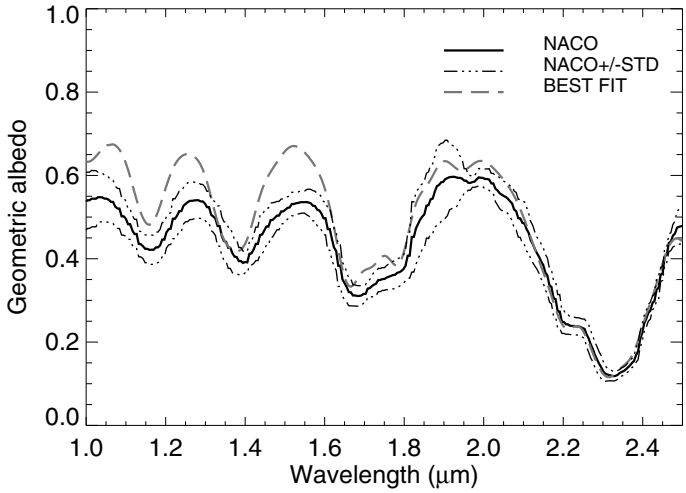

Fig. 7. Comparison between the averaged NACO spectrum of Pluto (solid line), including STD (dash dot dot dot line), and the best-fitting model (dashed line) degraded to the same spectral resolution as the NACO observations over the wavelength range (1–2.5) μm.

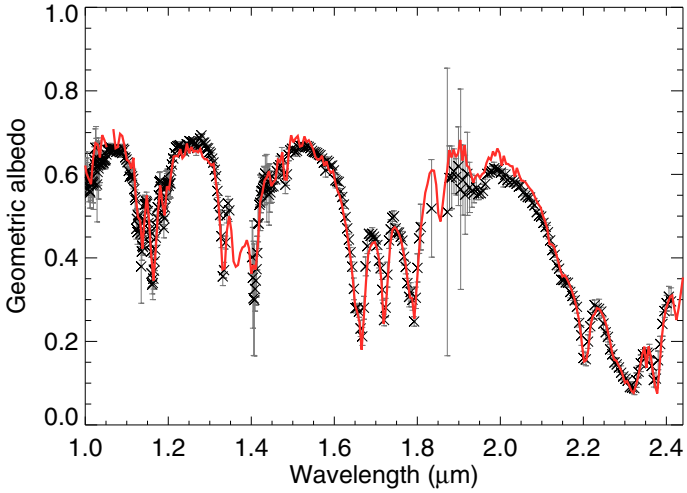

Fig. 8. IRTF observations (black crosses) (Olkin et al. 2007) compared with the best fitting model (red solid line) over the wavelength range (1.0–2.4) μm. (See the electronic version of the Journal for a color version of this figure.)

of Pluto's surface. Clearly, this possibility must be confirmed by further observations.

Another point of importance is the nature of the surface elements responsible for this slope variation. Many ices, such as H_2O, but also complex organics such as tholin-type radiolysis/photolysis residues (Khare et al. 1984, 1989; McDonald et al. 1994), absorb strongly in the region between 2.9 and 3.1 μm. Also, this slope is known to be diagnostic for the ratio between pure methane and methane diluted in nitrogen since the spectrum of pure methane presents a steeper slope than methane diluted in nitrogen (Olkin et al. 2007). This implies that considering a higher CH_4-CH_4:N_2 ratio than the one used to model the Keck spectrum would fit better the NACO observations. This latter approach was taken into consideration for this work. The best-fit model of the IRTF and Keck data in the wavelength range (1.0–2.4) μm and (2.9–3.7) μm was obtained with a three terrain unit model: 34% of CH_4 diluted in N_2 at 41 K with 95 mm grains (the concentration of CH_4 in N_2 is 0.36%), 37% of CH_4 at 60 K with 764 μm and 29% of Khare et al. (1984) titan tholin with 23 μm grains (Fig. 11). These values are different from those reported by Olkin et al. (2007) because of the use of a different phase function. Knowing of the coexistence of pure and diluted methane at the surface of Pluto (Douté et al. 1999), we tried to get a better fit of the slope of the NACO data by increasing only the abundance of pure methane in the mixture while maintaining that of diluted methane. Figure 12 shows the effect on the spectral model for various fractions of pure methane and using different grain sizes. In particular, it is evident that a model consisting of 34% of diluted methane and 37% of pure CH_4 (dashed green line) would not match the slope of the NACO spectrum of Pluto. Adding 15% of pure methane results in a steeper slope, which further increases when the grain sizes are reduced (see

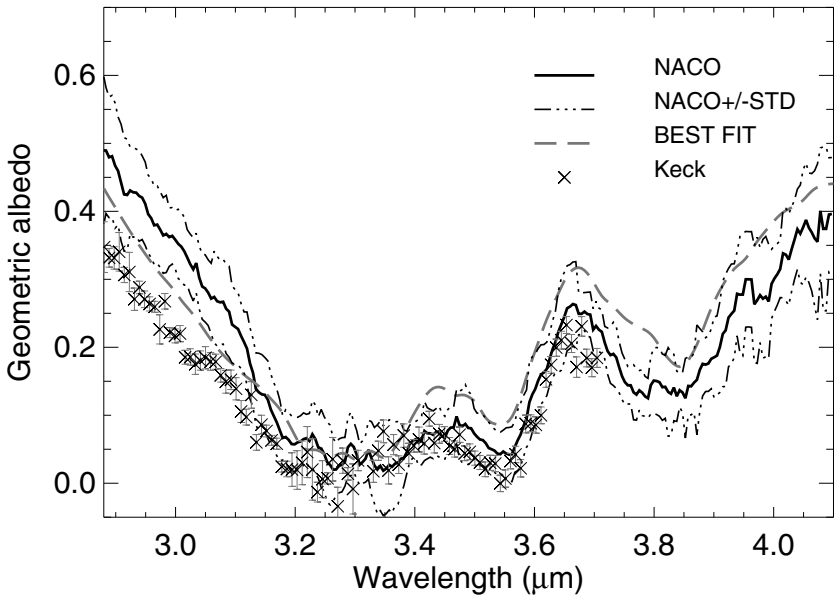

Fig. 9. Comparison between the averaged NACO spectrum of Pluto (solid line), including STD (dash dot dot dot line), and the best-fitting model (dashed line) over the wavelength range (2.9–4.1) μm. Overplotted are also Pluto's measurements (crosses) obtained with the Keck telescope in 2001 (Olkin et al. 2007).

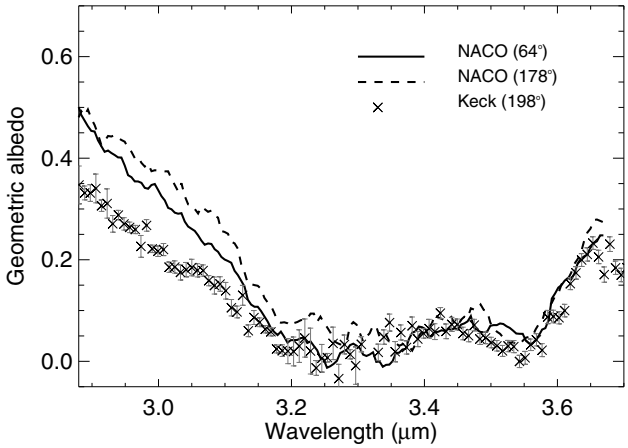

Fig. 10. Near infrared spectra of the two opposite hemispheres of Pluto (solid and dashed lines) obtained with NACO in 2005 compared to the observations obtained with the Keck telescope (crosses) in 2001 over the wavelength range (2.88–3.7) μm.

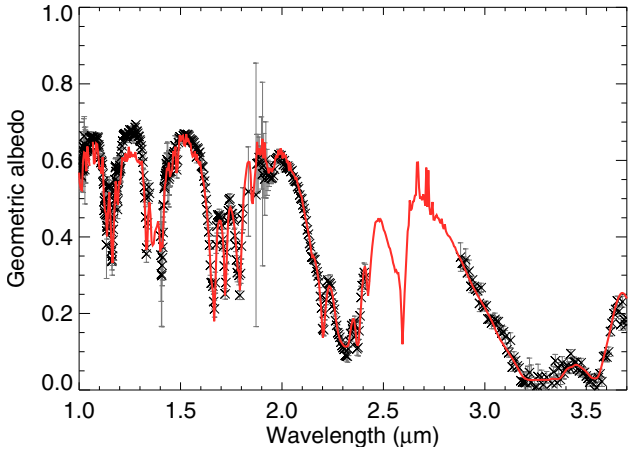

Fig. 11. IRTF and Keck observations (Olkin et al. 2007) over the wavelength range (1.00–2.40) μm and (2.88–3.70) μm, respectively (black crosses). Overplotted (red solid line) is our model of these observations. (See the electronic version of the Journal for a color version of this figure.)

dash dot blue and long dashed gray lines in Fig. 12). However, Fig. 12 shows that grain sizes smaller than 70 μm produce a synthetic spectrum (dash dot dot dot violet line) that is too narrow around 3.3 μm absorption dip (Olkin et al. 2007) and at the same time, it is too high around 3.55 and 3.80 μm (Olkin et al. 2007).

The compound that could contribute significantly to the absorption band at 4.6 μm is CO ice, which has an absorption band around 4.67 μm. Figure 13 shows the comparison between NACO spectrum (black solid line) and the best fitting model (dashed gray line), at the same spectral resolution as the observations. The insert box in Fig. 13 shows the contribution of the CO ice absorption band at 4.67 μm to the 4.6 μm feature in Pluto's spectrum over the wavelength range 4.4–5 μm. The comparison between NACO spectrum (black solid line) and the best fitting model obtained by including (dashed gray line) and removing (dash dot red line) the absorption band of CO ice at 4.67 μm is shown as well.

Another species that could contribute to Pluto's absorption band around 4.6 μm is CH_3D. The laboratory reflectance spectrum of pure CH_4 shows two absorptions, at 4.34 and 4.56 μm (see dashed and dash dot lines in Fig. 5). These absorptions do not correspond to any known CH_4 vibrational transition, and were tentatively attributed to CH_3D (Grundy et al. 2002b). Figure 13 (see insert box) shows the contribution of the 4.56 μm absorption of CH_3D to the fit of the observed 4.6 μm feature in Pluto's spectrum, presenting the comparison between the NACO spectrum (black solid line) and the best-fit model obtained by including (dashed gray line) and removing (dotted green line) the absorptions due to CH_3D. It is clear that the contribution of CH_3D to the Pluto feature in the M-band is almost negligible.

We investigated the possibility that nitriles might explain the 4.6 μm feature in the Pluto spectrum. Among the several nitriles studied in the lab (see Sect. 3.1), those having absorption bands near 4.6 μm are CH_2CHCN, C_2N_2 and CH_3CH_2CN.

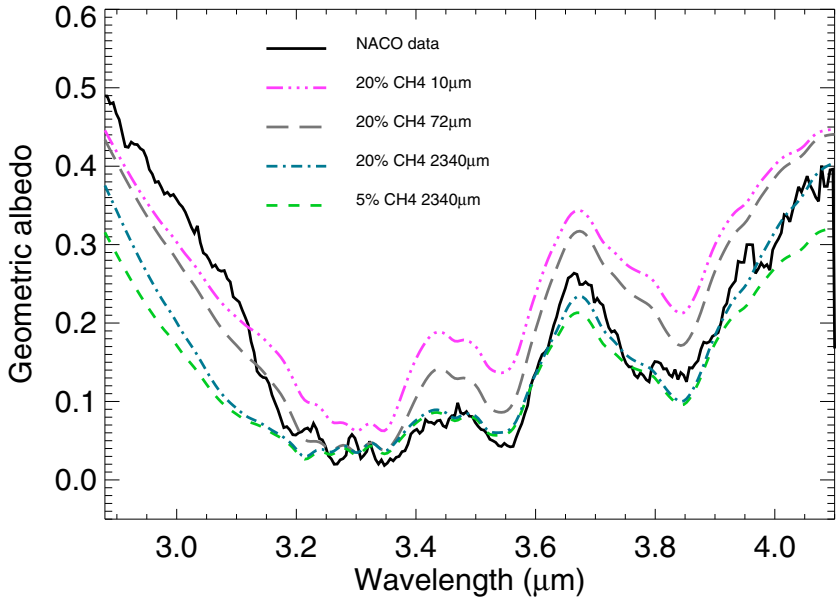

Fig. 12. Modeling results for different concentrations of pure methane and different grain sizes, compared with NACO L band spectrum of Pluto. By default, all the models assume 32% of pure CH_4 with 2340 μm grain size, 34% of CH_4 and CO ice diluted in N_2 with 95 mm grains, 6% of CH_2CHCN with 9 μm grains and 8% of titan tholin at 100 μm grains. Only the percentage of pure methane ice and its grain sizes are varied. The sensitivity of the *L* band spectrum to changes in the grain size of pure CH_4 is shown in the figure by some examples. (See the electronic version of the Journal for a color version of this figure.)

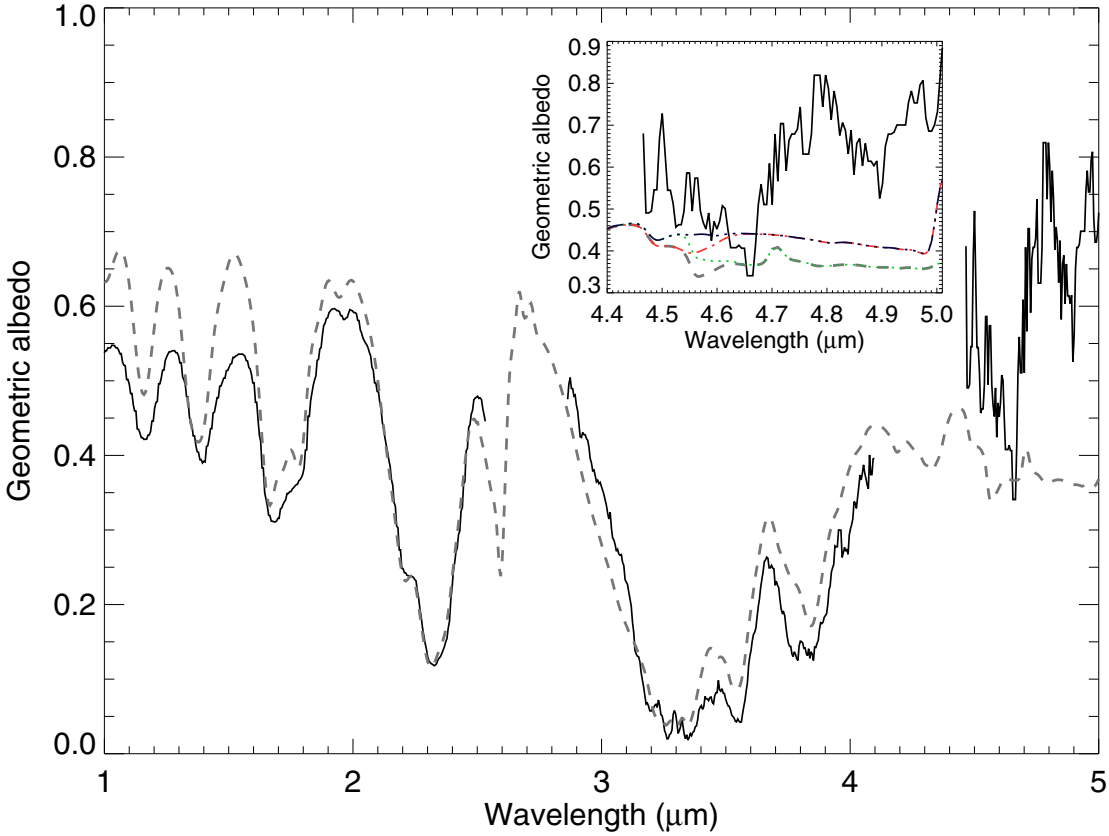

Fig. 13. Pluto's spectrum (solid black line) obtained by NACO with the best-fitting model (dashed gray curve), at the same spectral resolution as the observations, over the wavelength range (1–5) μm. In the insert box the comparison between NACO spectrum (black solid line) and the best fitting model obtained by including (dashed gray line) and removing (dash dot red line) the absorption band of CO ice at 4.67 μm over the wavelength range 4.4–5 μm is shown. The best fitting model obtained after removing the contribution of CH_3D at 4.34 and 4.56 μm (dotted green line) is also shown. The dash dot dot dot blue line represents the best-fitting model considering the contribution of CH_2CHCN only. (See the electronic version of the Journal for a color version of this figure.)

In spite of the fact that the width of the Pluto band suggests that it arises from a mixture of several different nitriles, we preferred to consider in the modeling only those having a band near 4.6 μm. Because of the difficulty in establishing a reliable continuum level around the 4.6 μm Pluto band, the actual width of the absorption remains uncertain, while its maximum depth seems to be better defined. In the modeling, we have investigated the effects of the mixture of both CH_2CHCN and C_2N_2, while CH_3CH_2CN was not taken into account because of the absence of optical constants. We found that acrylonitrile (see Fig. 5) is the only nitrile having an absorption around 4.6 μm that also gives a satisfactory fit to Pluto's spectrum in the short wavelength region. However, the introduction of CH_2CHCN results only in a weak absorption (weaker than the feature detected), and furthermore this absorption is located to the left (4.5 μm) of the detected 4.6 μm Pluto band (see Fig. 13, dash dot dot dot blue line in the insert box). Adding C_2N_2 in the mixture, the model diverges from the observed spectrum around 3.3 μm with albedo values higher than those observed.

4.2. Charon

One of the best spectroscopic models proposed for Charon is the "standard model" by Buie & Grundy (2000). The model assumes an intimate mixture of 60% H_2O with 100 μm grain size and 40% of a neutral continuum absorber with 70 μm grains. The optical constants of the absorber were calculated by Buie & Grundy (2000) in the wavelength range (0.44–2.6) μm in order to match the HST/NICMOS data from 1.4 to 2.5 μm. We extended the "standard model" beyond 2.6 μm, assuming the neutral absorber has a flat spectrum in the range from 2.6 to 4.1 μm (with an absorption coefficient of 822 cm^{-1}). Figure 14 shows Charon's spectrum (solid line), normalized in the wavelength range (2.2–2.3) μm to 0.27, corresponding to Charon's reflectance at 1° phase angle, named A_1 in agreement with Buie & Grundy (2000). The figure also shows the comparison between the NACO spectrum of Charon and the "standard model" extrapolated beyond 2.6 μm (dashed line) for the wavelength range (1.0–4.1) μm. As for Pluto, the model deviates from the observations in the short wavelength region between 1.0 and 1.4 μm because of the light loss in the NACO spectrum due to the atmospheric refraction. Figure 15 shows the average Charon spectrum (solid line) together with its standard deviation (STD) as function of wavelength (dash dot dot dot lines) compared with the model (dashed line) in the wavelength regions (1.0–2.5) μm (top panel) and (3.0–4.1) μm (bottom panel). The deviation of the extrapolated "standard model" from the NACO data is still within the uncertainties of the measurements. However, the assumption that the neutral absorber is "flat" also between 2.6 and 4.1 μm results in albedo values that are systematically lower than those observed, at least beyond 3.2 μm. This discrepancy in the L band between the Charon spectrum and the extrapolated "standard model" suggests that the neutral absorber may probably absorbs less beyond 3.2 μm than anticipated. Figure 16 shows the comparison between Charon's spectrum (solid line) and the standard model (dashed line) now with the assumption that the absorption coefficient of the neutral absorber is 822 cm^{-1} in the range (2.7–3.2) μm, 150 cm^{-1} in the range (3.3–3.7) μm and 100 cm^{-1} from 3.8 to 4.1 μm. The match of the NACO data is improved. However, since the optical constants of the absorber are adopted (and not measured) only, no firm conclusion can be drawn from these results. Figure 17 shows the comparison between the geometric albedo of Pluto-Charon ($A_{g\mathrm{PC}}(\lambda)$) combined (solid line) and that of Pluto ($A_{g\mathrm{P}}(\lambda)$) only (dashed line) over

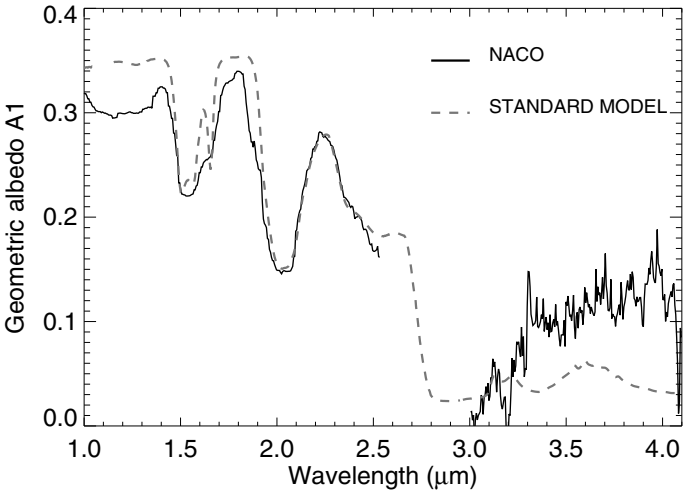

Fig. 14. Charon's spectrum at 1° phase angle (A_1) obtained with NACO in the wavelength range (1.0–4.1) μm (solid line) compared with the "standard model" of Buie & Grundy (2000) extrapolated beyond 2.6 μm (dashed curve) as described in the text. The feature around 3.2 μm is maybe an artifact from the data reduction.

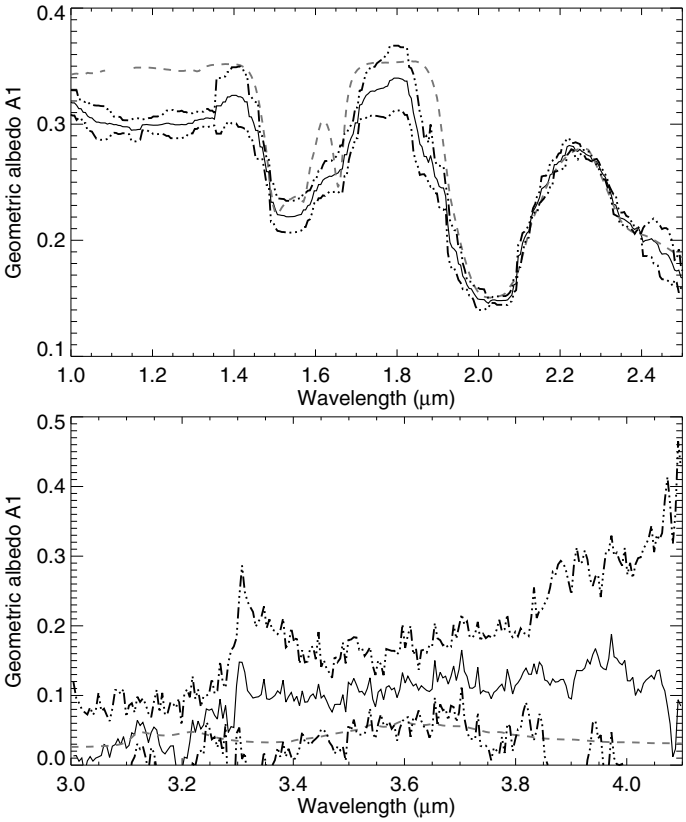

Fig. 15. Comparison between the averaged NACO spectrum (solid) together with its STD (dash dot dot dot) and the extended "standard model" (dashed) over the wavelength range (1.0–2.5) μm (*top panel*) and (3.0–4.1) μm (*bottom panel*).

the wavelength range (1.0–4.1) μm. The former was calculated using the following formula

$$A_{g\mathrm{PC}}(\lambda) = \frac{F_{\mathrm{PC}}(\lambda)}{F_{\mathrm{P}}(\lambda)} A_{g\mathrm{P}}(\lambda) \quad (3)$$

where $F_{\mathrm{PC}}(\lambda)$ and $F_{\mathrm{P}}(\lambda)$ indicate the relative reflectances of Pluto/Charon system and Pluto, respectively. The previous

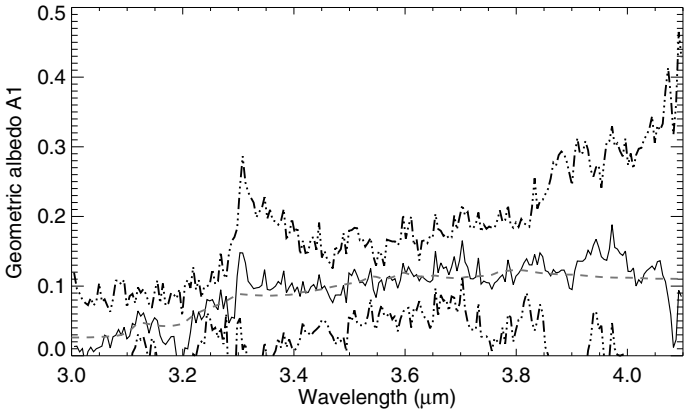

Fig. 16. Comparison between the averaged spectrum of Charon (solid) together with its STD (dash dot dot dot) and the "standard model" (dashed), now modifying the absorption coefficient of the neutral continuum absorber in the wavelength region beyond 3.2 μm (see text).

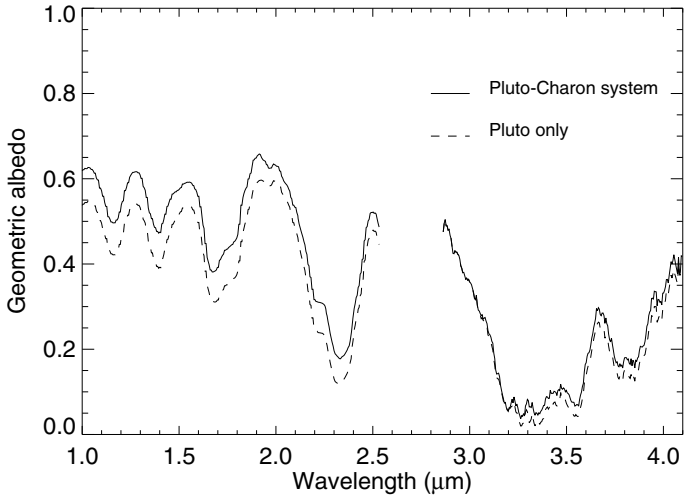

Fig. 17. Geometric albedo of Pluto-Charon system (solid line) compared with the one of Pluto alone (dashed line) in the wavelength range (1.0–4.1) μm.

relation was obtained from Eq. (2) of Douté et al. (1999) using the heliocentric distance, geocentric distance and mean quadratic radius of Pluto/Charon system the same as those of Pluto. The difference between the averaged geometric albedo of the combined system and that of Pluto represents Charon's spectral contribution to the unresolved system. This results in a contribution of 7% in *JHK* and about 2% in the *L*-band.

5. Conclusions

We have obtained the first resolved Pluto and Charon spectra up to 5 μm and 4 μm, respectively. These data provide important tools to improve our knowledge of the surfaces of Pluto and Charon.

The *M*-band spectrum of Pluto reveals the presence of an absorption band around 4.6 μm not previously detected. We found that CO ice, known to be present on Pluto's surface from the short wavelength region, contributes significantly to this feature, showing an absorption band at 4.67 μm. We investigated the possibility that nitriles on Pluto might be the explanation for the 4.6 μm band we find. Nitriles are not unexpected because they are products of reactions between methane and nitrogen (dello Russo & Khanna 1996), both species present on the surface of Pluto. In particular we found that acrylonitrile, CH_2CHCN, is the only nitrile having an absorption around 4.6 μm that also gives a satisfactory fit to Pluto's spectrum in the short wavelength region. We note, however, that the introduction of CH_2CHCN in our model results only in a weak absorption (weaker than the feature detected), and furthermore that this absorption is located to the left (4.5 μm) of the feature detected in Pluto's spectrum. Another species that weakly contributes to the 4.6 μm absorption in Pluto's spectrum, is deuterated methane, CH_3D, that has an absorption band at 4.56 μm, thus giving some hope for the eventual determination of the H/D ratio on Pluto. Unfortunately, lab data for the optical constants of CH_4 ice with various values of the H/D ratio are lacking (Grundy et al. 2002b) and the issue of the H/D ratio in Pluto remains unsolved for the time being.

Comparing the Pluto observations obtained at VLT in 2005 with those obtained at Keck in 2001, we note a significant change of the slope between 2.9 and 3.1 μm. Since different viewing longitudes is an unlikely explanation, one could consider instead changes in the observed Pluto's sub-solar latitude or a resurfacing process on Pluto, a hypothesis that clearly needs to be confirmed by further observations. The slope of the spectrum between 2.9 and 3.1 μm is diagnostic of the areal mixing ratio of pure to diluted CH_4, since pure CH_4 has a steeper slope than that of methane diluted in N_2. The modeling analysis of the NACO and Keck observations revealed that the concentration of pure CH_4 may have increased by 15% from 2001 to 2005.

Charon's spectrum obtained by NACO in 2005, is not contaminated by light from Pluto and extends well beyond 2.6 μm (compared to previous work by Buie & Grundy (2000) in the range (0.44–2.60) μm). Prior to the present study, Pluto's spectrum alone has been derived by removing a modeled spectrum of Charon from the ground-based spectra of the combined Pluto-Charon system (Olkin et al. 2007). Because of the absence of reflectance measurements for Charon beyond 2.5 μm, it was necessary to make assumptions about Charon's *L*-band spectrum. We have verified that the "standard model" of Buie & Grundy (2000), extended beyond 2.6 μm assuming that the absorption coefficient of the neutral absorber is 822 cm^{-1} in the range 2.6–4.1 μm, matches Charon's spectrum within the errors – although the modeled albedo is systematically lower than the measured value beyond 3.2 μm. Using NACO measurements for Charon it was possible to calculate the hypothetical spectral properties of the unknown neutral absorber beyond 2.6 μm to compensate for this deviations. The possible presence of hydrated ammonia on Charon's surface (Cook et al. 2007) was not taken into account, because the low spectral resolution of NACO data does not enable us to constrain the existence of this ice in Pluto's satellite.

Acknowledgements. We thank Chris Lidman and Nancy Ageorges, VLT staff astronomers and ESO faculty members, for their important help in the initial data analysis. Important contributions to this work were also made by many people who provided optical constants required for the modeling analysis, i.e. namely: A. Migliorini, J. Blum, C. Dalle Ore, C. de Bergh, N. Dello Russo, E. Quirico, T. L. Roush, B. Schmitt. We are grateful to J. Emery for sharing Spitzer results of Pluto-Charon as a private communication. We thank the referee of this paper for important comments and suggestions.

References

Barucci, M. A., Cruikshank, D. P., Dotto, E., et al. 2005, A&A, 439, L1
Brown, M. E., & Calvin, W. M. 2000, Science, 287, 107
Brown, M. E., Trujillo, C. A., & Rabinowitz, D. L. 2005, ApJ, 635, L97
Brown, M. E., Barkume, K. M., Blake, G. A., et al. 2007, AJ, 133, 284
Buie, M. W., & Grundy, W. M. 2000, Icarus, 148, 324
Buie, M. W., Tholen, D. J., & Wasserman, L. H. 1997, Icarus, 125, 233

Cook, J. C., Desch, S. J., Roush, T. L., Trujillo, C. A., & Geballe, T. R. 2007, ApJ, 663, 1406
Cruikshank, D. P., Pilcher, C. B., & Morrison, D. 1976, Science, 194, 835
Cruikshank, D. P., Allamandola, L. J., Hartmann, W. K., et al. 1991, Icarus, 94, 345
Cruikshank, D. P., Roush, T. L., Owen, T. C., et al. 1993, Science, 261, 742
dello Russo, N., & Khanna, R. K. 1996, Icarus, 123, 366
Douté, S., Schmitt, B., Quirico, E., et al. 1999, Icarus, 142, 421
Dumas, C., Merlin, F., Barucci, M. A., et al. 2007, A&A, 471, 331
Ehrenfreund, P., Boogert, A. C. A., Gerakines, P. A., et al. 1996, A&A, 315, L341
Grundy, W. M., & Buie, M. W. 2001, Icarus, 153, 248
Grundy, W. M., & Buie, M. W. 2002, Icarus, 157, 128
Grundy, W. M., Buie, M. W., & Spencer, J. R. 2002a, AJ, 124, 2273
Grundy, W. M., Schmitt, B., & Quirico, E. 2002b, Icarus, 155, 486
Hapke, B. 1993, Theory of reflectance and emittance spectroscopy (Topics in Remote Sensing, Cambridge, UK: Cambridge University Press)
Hillier, J., Veverka, J., Helfenstein, P., & Lee, P. 1994, Icarus, 109, 296
Horne, K. 1986, PASP, 98, 609
Khare, B. N., Sagan, C., Arakawa, E. T., et al. 1984, Icarus, 60, 127
Khare, B. N., Thompson, W. R., Murray, B. G. J. P. T., et al. 1989, Icarus, 79, 350
Krasnopolsky, V. A., & Cruikshank, D. P. 1999, J. Geophys. Res., 104, 21979
Licandro, J., Grundy, W. M., Pinilla-Alonso, N., & Leisy, P. 2006a, A&A, 458, L5
Licandro, J., Pinilla-Alonso, N., Pedani, M., et al. 2006b, A&A, 445, L35
Masterson, C. M., & Khanna, R. K. 1990, Icarus, 83, 83
McDonald, G. D., Thompson, W. R., Heinrich, M., Khare, B. N., & Sagan, C. 1994, Icarus, 108, 137
Merlin, F., Alvarez, A., Barucci, M., et al. 2007, in AAS/Division for Planetary Sciences Meeting Abstracts, Vol. 39
Olkin, C. B., Young, E. F., Young, L. A., et al. 2007, AJ, 133, 420
Owen, T. C., Roush, T. L., Cruikshank, D. P., et al. 1993, Science, 261, 745
Palumbo, M. E., & Strazzulla, G. 1993, A&A, 269, 568
Quirico, E., & Schmitt, B. 1997, Icarus, 127, 354
Quirico, E., Schmitt, B., Bini, R., & Salvi, P. R. 1996, Planet. Space Sci., 44, 973
Quirico, E., Doute, S., Schmitt, B., et al. 1999, Icarus, 139, 159
Schmitt, B., Quirico, E., & Lellouch, E. 1992, in Symposium on Titan, ed. B. Kaldeich, ESA SP, 338, 383
Spencer, J. R., Buie, M. W., & Bjoraker, G. L. 1990, Icarus, 88, 491
Szokoly, G. P. 2005, A&A, 443, 703
Tegler, S. C., Grundy, W. M., Romanishin, W., et al. 2007, AJ, 133, 526
Tegler, S. C., Grundy, W. M., Vilas, F., et al. 2008, Icarus, 195, 844